ACS APPLIED POLYMER MATERIALS

pubs.acs.org/acsapm

Article

Antimicrobial Nanogels with Nanoinjection Capabilities for Delivery of the Hydrophobic Antibacterial Agent Triclosan

Guangyue Zu, Magdalena Steinmüller, Damla Keskin, Henny C. van der Mei, Olga Mergel,* and Patrick van Rijn*

Cite This: *ACS Appl. Polym. Mater.* 2020, 2, 5779−5789

Read Online

ACCESS | Metrics & More | Article Recommendations | Supporting Information

ABSTRACT: With the ever-growing problem of antibiotic resistance, developing antimicrobial strategies is urgently needed. Herein, a hydrophobic drug delivery nanocarrier is developed for combating planktonic bacteria that enhances the efficiency of the hydrophobic antimicrobial agent, Triclosan, up to a 1000 times. The poly(*N*-isopropylacrylamide-*co*-*N*-[3-(dimethylamino)-propyl]methacrylamide), p(NIPAM-*co*-DMAPMA), based nanogel is prepared via a one-pot precipitation polymerization, followed by quaternization with 1-bromododecane to form hydrophobic domains inside the nanogel network through intraparticle self-assembly of the aliphatic chains (C12). Triclosan, as the model hydrophobic antimicrobial drug, is loaded within the hydrophobic domains inside the nanogel. The nanogel can adhere to the bacterial cell wall via electrostatic interactions and induce membrane destruction via the insertion of the aliphatic chains into the cell membrane. The hydrophobic antimicrobial Triclosan can be actively injected into the cell through the destroyed membrane. This approach dramatically increases the effective concentration of Triclosan at the bacterial site. Both the minimal inhibitory concentration and minimal bactericidal concentration against the Gram-positive bacteria *S. aureus* and *S. epidermidis* decreased 3 orders of magnitude, compared to free Triclosan. The synergy of physical destruction and active nanoinjection significantly enhances the antimicrobial efficacy, and the designed nanoinjection delivery system holds great promise for combating antimicrobial resistance as well as the applications of hydrophobic drugs delivery for many other possible applications.

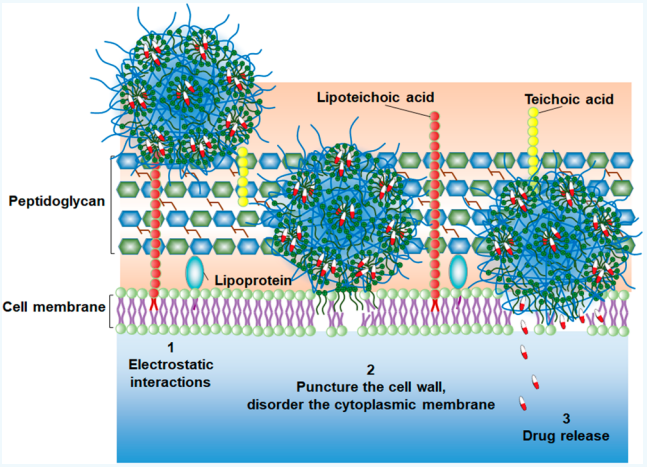

KEYWORDS: *antimicrobial, nanogels, drug delivery, quaternary ammonium, nanocarriers*

INTRODUCTION

Bacteria can cause life-threatening human diseases and lead to the death of 700 000 people annually worldwide.[1] This number is expected to rise in the coming years, as traditional antibiotics—the most widely used therapy to treat bacterial infections—are becoming less efficient due to the development of drug-resistant bacterial strains.[2−5] Thus, the necessity to overcome these challenges by developing antimicrobial agents and more effective delivery systems is of high importance.

The use of nanoparticles (NPs) is among the most promising strategies to overcome microbial drug resistance due to their diverse antimicrobial mechanism of action.[6] To date, many metal-based NPs exhibit inherent antibacterial activity; for instance, silver nanoparticles are widely explored as antibacterial agents.[7−9] However, the high cytotoxicity of metal-containing NPs is disadvantageous and limits their applicability.[10,11] Therefore, metal-free NPs, e.g., graphene materials,[12,13] cationic peptides,[14,15] polymer-based NPs,[16] and carbon quantum dots,[17] have drawn much attention recently. In particular, NPs functionalized with positively charged compounds can improve the attraction to the bacterial membrane and induce severe membrane rupture and subsequent cell death.[14]

Quaternary ammonium compounds (QACs), well-known cationic compounds, have been applied in the medical field as antimicrobial agents due to their broad-spectrum biocidal ability.[18] They contain a permanent positively charged fully alkylated nitrogen of which one is often a long alkyl chain. The mechanism of action of QACs against bacteria was proposed to first entail the attraction of the positively charged cationic head to the negatively charged bacterial cell surface by electrostatic

Received: September 16, 2020
Accepted: November 4, 2020
Published: November 11, 2020

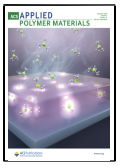

https://dx.doi.org/10.1021/acsapm.0c01031
ACS Appl. Polym. Mater. 2020, 2, 5779−5789

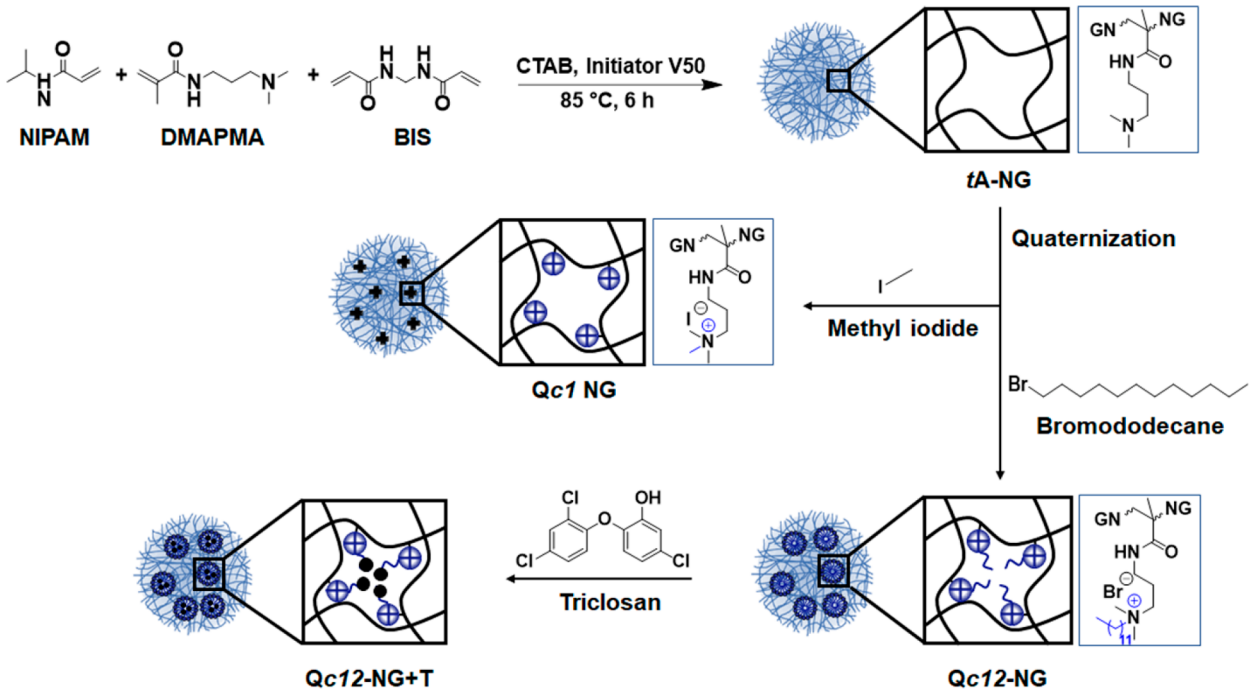

Figure 1. Schematic illustration of the main synthesis procedure of the antimicrobial nanogels. The tertiary amine-functionalized nanogel (*t*A-NG) was synthesized by precipitation polymerization of NIPAM with DMAPMA. The quaternized nanogels (Q*cn*-NG (*n* = 1 or 12)) were prepared by functionalization of the tertiary amine group with different alkyl chain lengths of quaternization agents (methyl iodide and 1-bromododecane). Finally, the Triclosan-loaded nanogel (Q*c12*-NG+T) was obtained by loading the antimicrobial agent Triclosan in the Q*c12*-NG via the hydrophobic interaction between Triclosan and the hydrophobic cavity inside nanogel networks formed by the alkyl chain (C12).

interactions, penetrate through the peptidoglycan layer, and then disrupt the lipids membrane of Gram-positive bacteria through the hydrophobic interaction by the hydrophobic alkyl chain.[19,20] This interaction causes membrane destabilization and the subsequent leakage of cytoplasmic compounds.[21−24] QACs cause in general more damage to bacteria than to the membranes of mammalian cells.[25] Therefore, QACs are consequently mostly applied as contact-killing coatings on surfaces to combat bacterial infections.[26−28] However, there are only a few works that address the application of QACs-functionalized NPs to kill bacteria in suspension.[29−31] Zhang and co-workers developed a series of quaternized fluorescent silicon NPs as antibacterial agents with both bacterial imaging and killing capability.[32] However, it was observed that the antimicrobial properties of QACs highly depend on the length of the alkyl chain.[33] The longer the chain (up to a maximum number of carbons between 12 and 16), the higher the tendency for the molecule to intercalate into the membrane of the bacteria, but the lower the aqueous solubility,[34] which limited the application of QACs to eradicate bacteria under physiological conditions.

Another strategy to overcome resistance is to improve delivery or accessibility of existing bactericides to enhance the effectiveness at the lesion site, especially of the hydrophobic drugs, which have poor solubility and bioavailability.[35] For example, Triclosan, a commercial broad-spectrum hydrophobic antimicrobial, combats bacteria by nonspecific interaction with the cell membrane leading to the death of bacteria but also specifically blocks the lipid synthesis to stop the bacterial growth.[36]

To overcome the limiting factors mentioned above, nanogels stand out because of their unique properties. Nanogels are "smart" nanomaterials with many advantages and possibilities.[37,38] The enormous interest in these smart polymers is illustrated by their wide field of potential applications due to the stimuli responsiveness and the ability to undergo a volume phase transition (VPT) concerning environmental changes.[39−41] These soft and deformable polymeric particles consist of a cross-linked and porous network, which can be functionalized with various functional groups to introduce catalytic activity,[42] antifouling property,[43,44] or selective permeability[45] but also have been used to implement antimicrobial groups and specific ligands.[46,47] Their high surface to volume ratio, high degree of functionalization, and hence multivalency on the nanoparticle surface are advantageous for interactions with bacteria[48] as the deformability of the soft particles ensures a high contact area in comparison to rigid nanoparticles.[38] Moreover, nanogels are ideal drug-delivery carriers due to their excellent drug-loading capacity, high stability, and good biocompatibility.

Therefore, in our study, a poly(*N*-isopropylacrylamide-*co*-*N*-[3-(dimethylamino)propyl]methacrylamide) (p(NIPAM-*co*-DMAPMA)) based nanogel quaternized with 1-bromododecane was designed to induce intraparticle micellization and thereby create a hydrophobic environment inside the nanogel network. Triclosan, as a model hydrophobic drug, was loaded into the nanogel by hydrophobic interactions to increase the effective concentration dramatically at the bacterial site that is otherwise beyond reach. To assess the antimicrobial efficacy of the prepared nanogels, the minimum inhibitory concentration (MIC) and minimum bactericidal concentration (MBC) against Gram-positive model bacteria *Staphylococcus aureus* (*S. aureus*) and *Staphylococcus epidermidis* (*S. epidermidis*), two of the most important pathogens in nosocomial infections

https://dx.doi.org/10.1021/acsapm.0c01031
ACS Appl. Polym. Mater. 2020, 2, 5779−5789

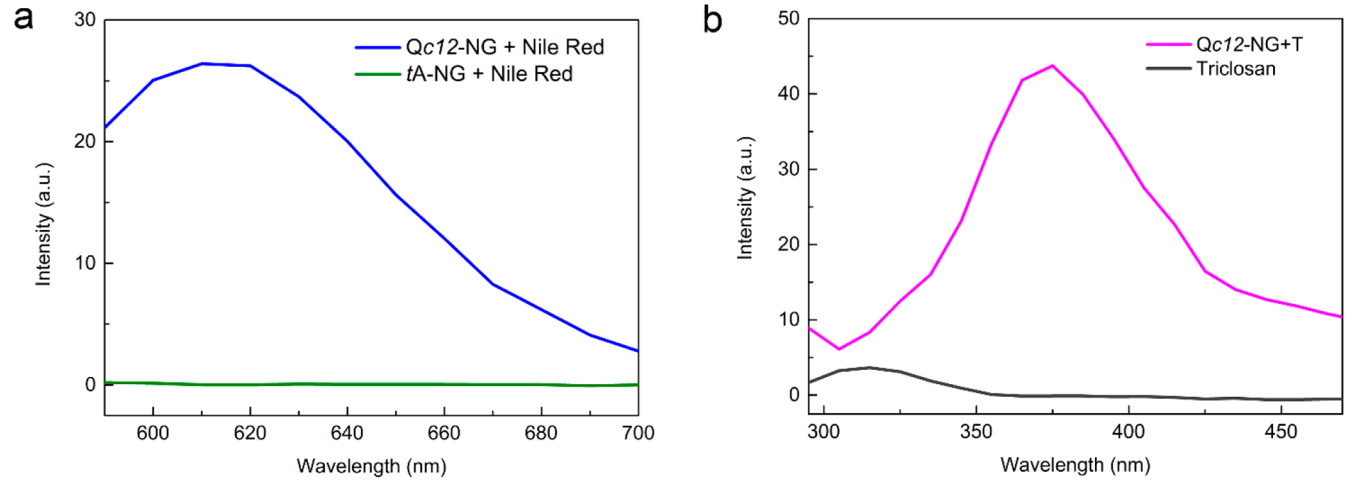

Figure 2. Fluorescence spectra of (a) Nile Red in the presence of dodecyl-quaternized nanogel Q*c12*-NG and tertiary amine-functionalized nanogel *t*A-NG (excitation wavelength: 540 nm) and (b) Triclosan and Triclosan-loaded nanogel Q*c12*-NG+T (excitation wavelength: 280 nm).

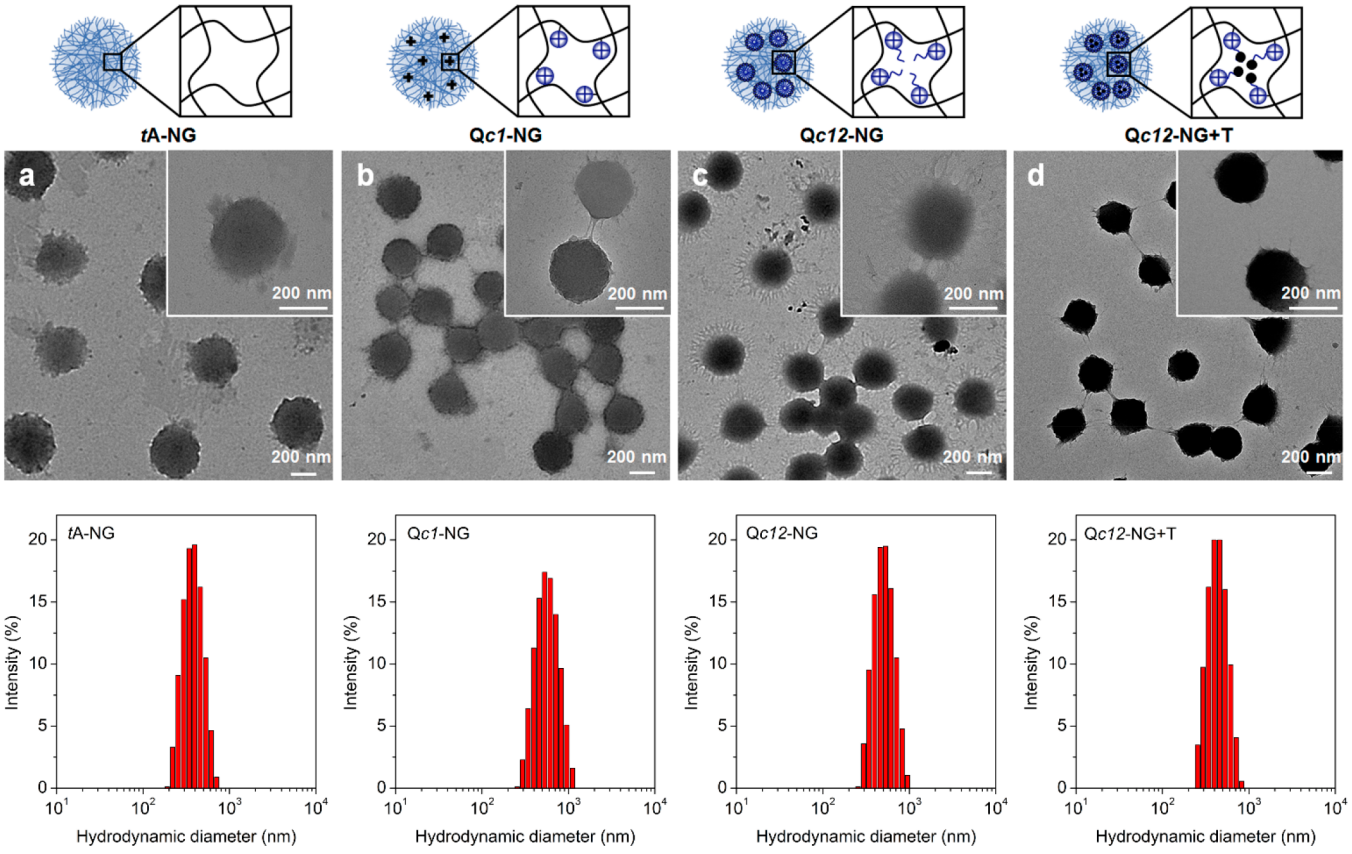

Figure 3. Transmission electron microscopy images of nanogels dried on a carbon-coated copper grid and size distribution by the intensity of nanogels in aqueous media determined by dynamic light scattering analysis in water at 25 °C. (a) Tertiary amine-functionalized nanogel *t*A-NG, (b) methyl-quaternized nanogel Q*c1*-NG, (c) dodecyl-quaternized nanogel Q*c12*-NG, and (d) Triclosan-loaded nanogel Q*c12*-NG+T (scale bar = 200 nm).

associated with catheters and other medical implants,[49,50] were determined. Moreover, we hypothesized that the combination of cell membrane disruption by the aliphatic chain and the "injection" of Triclosan would induce a synergistic effect and provide a system that kills bacteria more efficiently. Therefore, through the rational design of the nanogel delivery system, we could obtain a synergistic effect of both QACs and hydrophobic antimicrobial agents, thus reducing the amount of antimicrobials required to treat infections and, additionally, preventing the potential occurrence of drug resistance bacteria in the antimicrobial agents used.

RESULTS AND DISCUSSION

Preparation and Characterization of Quaternized Nanogels. For the formation of the antimicrobial nanogels, first, a tertiary amine-functionalized nanogel (*t*A-NG) was

https://dx.doi.org/10.1021/acsapm.0c01031
ACS Appl. Polym. Mater. 2020, 2, 5779−5789

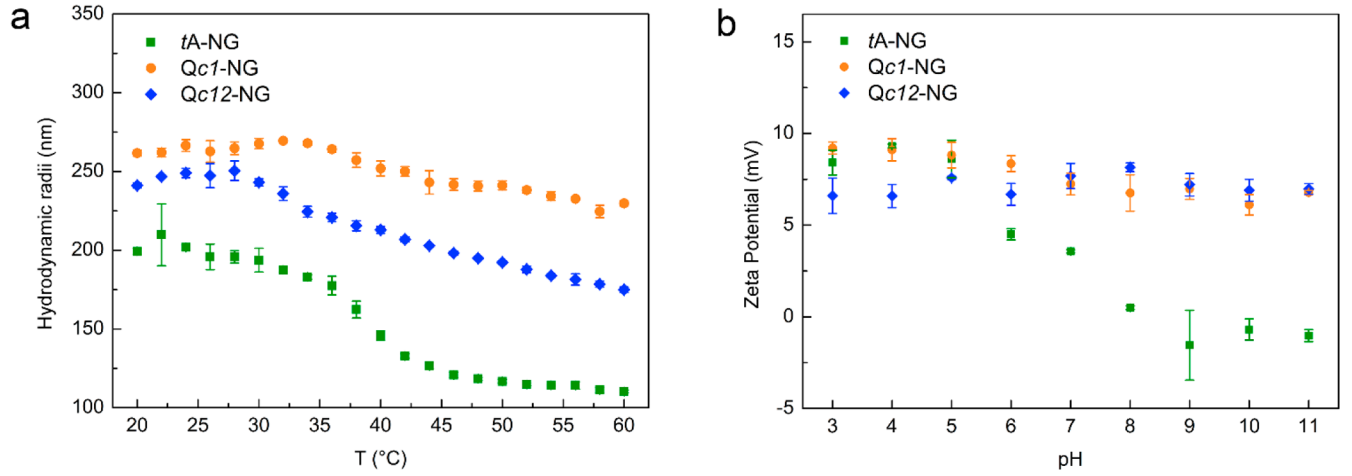

Figure 4. (a) Hydrodynamic radii as a function of temperature obtained from dynamic light scattering measurements for tertiary amine-functionalized nanogel *t*A-NG, methyl-quaternized nanogel Q*c1*-NG, and dodecyl-quaternized nanogel Q*c12*-NG in water. (b) pH-dependent zeta potential of the *t*A-NG, Q*c1*-NG, and Q*c12*-NG in 0.05 M NaCl at 25 °C.

synthesized via precipitation polymerization. For the reaction, the thermoresponsive monomer NIPAM and the pH-responsive comonomer DMAPMA were used of which the latter contains the tertiary amine group required for the quaternization, as shown in Figure 1. The molar ratio of tertiary amine to NIPAM within *t*A-NG as determined by quantitative analysis using ^{1}H NMR is 12 mol % related to NIPAM (Figure S1), which is in good agreement with the monomer feed ratio adjusted during the synthesis (11.8 mol % of DMAPMA related to NIPAM). To obtain the antimicrobial properties, the tertiary amine functionality within the nanogel was quaternized by alkylating the tertiary amine groups with 1-bromododecane (Q*c12*-NG) and methyl iodide (Q*c1*-NG), respectively, as shown in Figure 1. The numbers C1 and C12 indicate the length of the carbon chain used for the quaternarization, and Q*c1*-NG is considered as the control nanogel to indicate the effect of the positive charge without the presence of the longer aliphatic chain conventionally required to ascertain the antimicrobial property. The degree of quaternization is approximately 78% of Q*c1*-NG and 94% of Q*c12*-NG, calculated from quantitative ^{1}H NMR analysis of the nanogels before and after quaternization (Figure S1).

Characterization of Triclosan-Loaded Nanogels. In designing the nanogel constructs, the hydrophobic moieties of Q*c12*-NG are responsible for the antimicrobial effect. However, by inclusion of long aliphatic chains within a flexible hydrogel network, a hydrophobic environment due to intraparticle self-assembly (micellization) was generated. This intraparticle micelle formation could encapsulate hydrophobic components such as the hydrophobic antibacterial agent Triclosan to further increase the biocidal ability of the nanogel (Q*c12*-NG+T), as shown in Figure 1.

Before Triclosan was encapsulated into the nanogel, the hydrophobic cavity formation within Q*c12*-NG was determined by loading Nile Red, a bathochromic fluorescent dye conventionally used to determine the critical micelle concentration, and hydrophobic domains are indicated by a shift in the emission wavelength as well as an increase in the fluorescence intensity.[51,52] Both Q*c12*-NG and *t*A-NG without aliphatic chains were incubated with Nile Red. The fluorescence spectra were collected, and the results are shown in Figure 2a. The maximum emission wavelength of Nile Red-loaded Q*c12*-NG was observed to be around 610 nm (540 nm excitation), while no fluorescence emission was observed for Nile Red in the presence of the *t*A-NG. The fluorescence properties of Nile Red are highly sensitive to the environment where it is located.[53] The fluorescence intensity is very weak in aqueous medium, a polar solvent, but increases drastically in a hydrophobic environment.[54] Therefore, the results shown in Figure 2a suggest that hydrophobic cavities are present and generated by the aliphatic chains within the hydrophilic network of the nanogel.

The loading of Triclosan was also detected with fluorescence spectroscopy. As shown in Figure 2b, the maximum emission wavelength of Q*c12*-NG+T was around 376 nm (280 nm excitation), while the Triclosan itself only showed a weak pronounced emission band around 315 nm, which is consistent with previous studies.[55] Triclosan is a lipophilic compound and has a weak fluorescence intensity in aqueous solution due to the poor solubility. However, the presence of Triclosan in a hydrophobic environment induced a high fluorescence intensity accompanied by a spectral red shift. Therefore, the results shown in Figure 2b indicate the successful loading of Triclosan into the Q*c12*-NG and further prove the formation of hydrophobic domains inside the nanogel. The Triclosan loading capacity of Q*c12*-NG+T was 6.3 wt %, measured by UV−vis spectroscopy (Figure S2).

Nanogel Morphology, Hydrodynamic Properties, and Behavior in Aqueous Media. Figure 3 shows representative transmission electron microscopy (TEM) images and hydrodynamic size distribution determined by dynamic light scattering analysis (DLS) of all investigated nanogels. The TEM micrographs revealed that all of the prepared nanogels were spherical in shape, monodisperse, and similar in size: 347 ± 30, 289 ± 27, 345 ± 22, and 268 ± 15 nm in diameter for *t*A-NG, Q*c1*-NG, Q*c12*-NG, and Q*c12*-NG+T, respectively. Independent of the quaternization with methyl iodide and 1-bromododecane and the drug loading of Triclosan, all the nanogels diameters displayed narrow size distributions as shown in Figure 3. Although the nanogels look very similar, the Q*c12*-NG displays a diffuse edge around the nanogel in the TEM image while after the encapsulating of Triclosan, the diameter was slightly decreased, and the nanogel appears less fuzzy. This effect may be attributed to the hydrophobic

https://dx.doi.org/10.1021/acsapm.0c01031
ACS Appl. Polym. Mater. 2020, 2, 5779−5789

Table 1. Minimal Inhibitory and Minimal Bactericidal Concentrations (MIC and MBC, Respectively) of *t*A-NG, Q*c1*-NG, Q*c12*-NG, Free Triclosan, and Encapsulated in Q*c12*-NG+T for *S. epidermidis* ATCC 12228, *S. epidermidis* HBH 45, *S. aureus* 5298, and *S. aureus* ATCC 12600

bacterial strain	μg mL^{-1}	*t*A-NG	Q*c1*-NG	Q*c12*-NG	triclosan	Q*c12*-NG+T[a] (loaded triclosan)	times more efficient (x)[b]
S. epidermidis ATCC 12228	MIC	>4000	>4000	500	1.25	0.00246	509
	MBC	>4000	>4000	1000	5	0.00983	509
S. epidermidis HBH 45	MIC	>4000	>4000	500	1.25	0.00491	254
	MBC	>4000	>4000	500	10	0.0394	254
S. aureus 5298	MIC	>4000	>4000	500	2.5	0.00246	1018
	MBC	>4000	>4000	1000	5	0.0246	203
S. aureus ATCC 12600	MIC	>4000	>4000	500	1.25	0.00491	254
	MBC	>4000	>4000	1000	10	0.0123	814

[a]Concentrations given are that of Triclosan. Note that in the case of MIC and MBC values against Triclosan-loaded nanogel, encapsulated Triclosan concentrations are derived from the nanogel concentration and the Triclosan loading content 6.3%. [b]x = MIC (Triclosan)/MIC (Q*c12*-NG+T) or MBC (Triclosan)/MBC (Q*c12*-NG+T).

moieties stored inside the hydrophobic domains and interaction with Triclosan and therefore creates a slightly denser matrix. The nanogel network is denser driven by the hydrophobic interaction. The TEM micrographs further suggest that the Triclosan was loaded into the nanogel via hydrophobic interactions within the hydrophobic domains of the nanogel.

To further identify the hydrodynamic properties and indicate the behavior within the aqueous media, the temperature- and pH-responsive behavior of the three different nanogels, *t*A-NG, Q*c1*-NG, and Q*c12*-NG, were measured using DLS. The tertiary amine-functionalized nanogel *t*A-NG is temperature responsive based on the poly-NIPAM segment, and the volume-phase transition temperature (VPTT) is around 38 °C, as shown in Figure 4a, which is consistent with previously reported work[56] and slightly higher than conventionally found for pure poly-NIPAM nanogels (around 32 °C).[57] The increase in VPTT is due to the incorporated comonomer DMAPMA, which is charged at neutral pH and increases the hydrophilicity of the polymer network causing electrostatic repulsion.[56] After quaternization with methyl iodide, the hydrodynamic radius (R_h) of the nanogel becomes slightly larger, and the temperature response is less pronounced due to stronger repulsive interactions. Due to the permanently charged ammonium moieties, there is no possibility for altering the protonation state; persistent electrostatic repulsion effectively counteracts the hydrophobic collapse, and a sharp decrease in R_h at a specific temperature is hindered. The nanogel collapse proceeds over a broad temperature range instead. The repulsive force among charged groups in the nanogel interior and the osmotic pressure of the counterions prevent a complete nanogel collapse.[58] However, in the case of dodecyl-quaternized nanogel, a slight decrease of the R_h with temperature was observed without a distinguishable VPTT. The reduction in size compared to the methyl-quaternized nanogel indicates that there is an internal attractive force that facilitates this size reduction, which is most likely the attraction of the hydrophobic aliphatic tails (micellization). There is less charge repulsion due to the internal reorganization of charges within the nanogel compared to methyl-quaternized nanogel, and therefore the temperature responsiveness is regained to some extent.

In addition, the comonomer DMAPMA also induced the pH responsiveness to the nanogel, as shown in Figure 4b. The zeta potential of *t*A-NG decreased from +8.4 to −1.0 mV with increasing pH and is around 0 mV above pH 10. With increasing pH, the tertiary amine groups of *t*A-NG become deprotonated until the nanogel is neutral between pH 8 and 9. After quaternization, the zeta potential of both Q*c1*-NG and Q*c12*-NG showed no pH responsiveness since the quaternary ammonium cations are permanently charged. The zeta potential of Q*c1*-NG only shows a slight decrease around pH 7, which is most likely due to the deprotonation of the remaining tertiary amine moieties since the quaternarization was about 78%.

Although not pertinent for the intended application, the changes in the behavior of the nanogels with aqueous media under different stimulating conditions show the effectiveness of the modifications and support the intraparticle micelle formation that is crucial for the storage of hydrophobic drugs and the delivery of these pharmaceutical agents. In addition, the change between room temperature and 37 °C for Q*c12*-NG is minimal, making it applicable for *in vivo* temperature conditions.

Antimicrobial Efficacy of the Nanogels. To investigate the bacterial inhibitory and killing effects of all the prepared nanogels, the minimal inhibitory concentration and minimal bactericidal concentration (MIC and MBC) of four different Gram-positive bacterial strains were determined (*S. epidermidis* ATCC 12228, *S. epidermidis* HBH 45, *S. aureus* 5298, and *S. aureus* ATCC 12600), and free Triclosan was introduced as a control. The results are shown in Table 1. Among the three nonloaded nanogels, both the tertiary amine-functionalized nanogel *t*A-NG and methyl-quaternized nanogel Q*c1*-NG showed no antimicrobial effect within the test concentration (4000 μg mL^{-1}), while the dodecyl-quaternized nanogel Q*c12*-NG displayed the potential antimicrobial activity against all the bacterial species. The MIC and MBC for Q*c12*-NG are 500 and 500 μg mL^{-1} for *S. epidermidis* HBH 45 and 500 and 1000 μg mL^{-1} for the other three strains, respectively. Compared to *t*A-NG, the quaternization with methyl iodide did not improve the biocidal activity of Q*c1*-NG, which indicates that the presence of a permanent positively charged quaternary ammonium group alone is not sufficient to kill bacteria. In order to be effective, the presence of the aliphatic chain is pertinent as used in the Q*c12*-NG, which can penetrate and disrupt cell membranes and results in the loss of membrane integrity with consequent leakage of essential intracellular constituents.[33]

All the bacterial strains have some susceptibility to the free antimicrobial drug Triclosan; the MIC are 2.5 μg mL^{-1} for *S. aureus* 5298 and 1.25 μg mL^{-1} for the other three strains. The

https://dx.doi.org/10.1021/acsapm.0c01031
ACS Appl. Polym. Mater. 2020, 2, 5779−5789

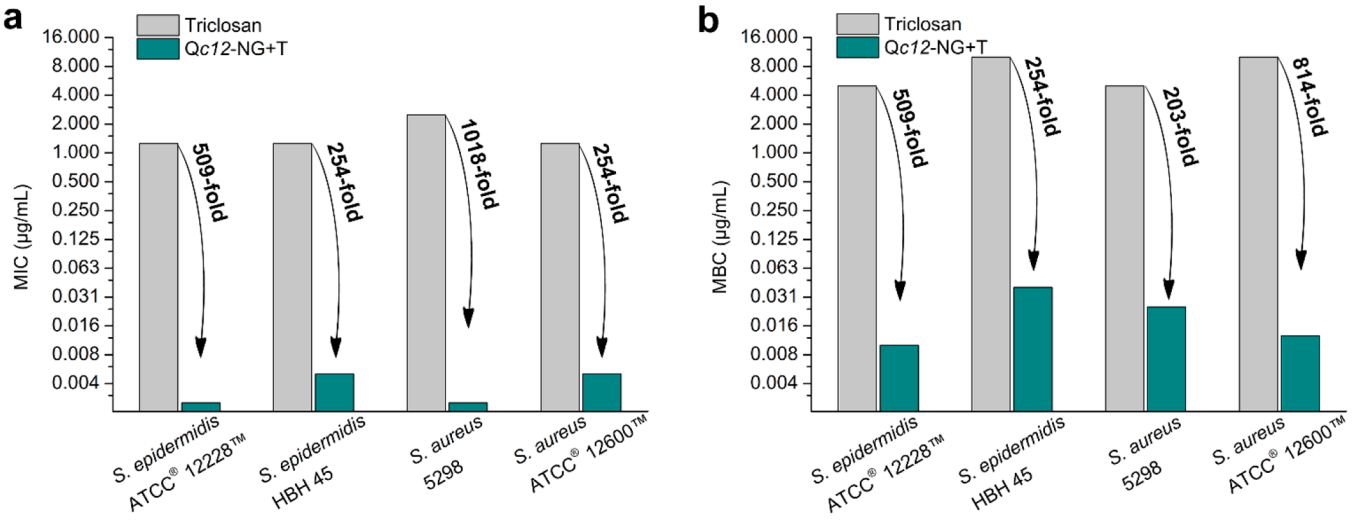

Figure 5. (a) MIC folds reduction and (b) MBC folds reduction of free Triclosan and encapsulated Triclosan in Q*c12*-NG+T for *S. epidermidis* ATCC 12228, *S. epidermidis* HBH 45, *S. aureus* 5298, and *S. aureus* ATCC 12600.

Scheme 1. Schematic Illustration of the Bactericidal Mechanism of Triclosan-Loaded Nanogel[a]

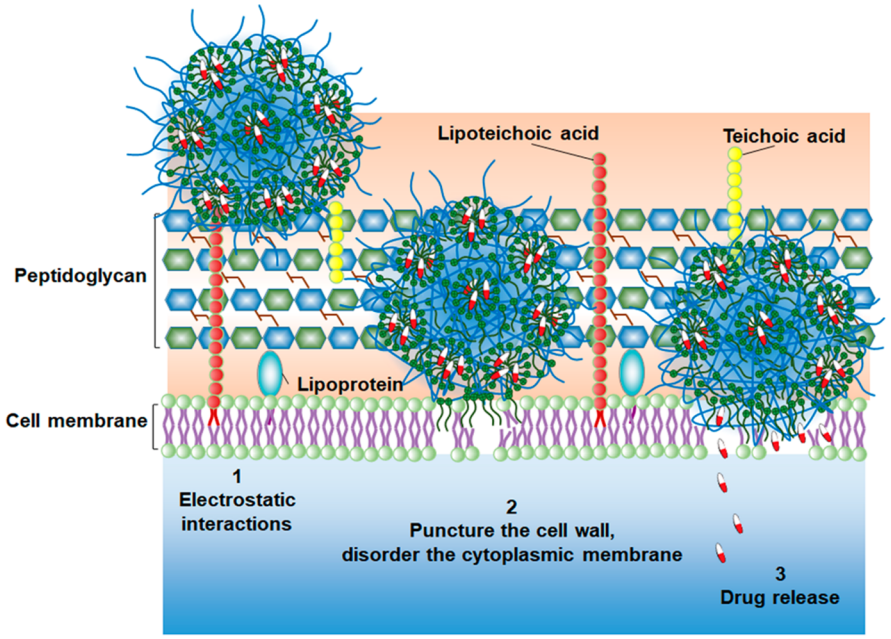

[a]Nanogels interact with the peptidoglycan and cell membrane layers of Gram-positive bacteria via electrostatic interactions (1) and kill the bacteria by puncturing the cell wall and disordering the cytoplasmic membrane (2), followed by the injection of Triclosan from the intraparticle micelles to the bacterial cell membrane and inside the cell (3).

required MBCs are two- to eightfold higher than MIC, which is consistent with previous work.[59] However, the Triclosan-loaded nanogel, Q*c12*-NG+T, displayed a tremendous enhancement in antimicrobial activity against all the bacterial strains. The MIC in terms of encapsulated Triclosan are 2.46 ng mL^{-1} for *S. epidermidis* ATCC 12228 and *S. aureus* 5298 and 4.91 ng mL^{-1} for *S. epidermidis* HBH 45 and *S. aureus* ATCC 12600, and the MBC required are four- to tenfold higher in concentration than MIC, which is a dramatic improvement compared to free Triclosan in aqueous solution. The concentrations are based on the available Triclosan present in the system. As shown in Figure 5, the MIC for Triclosan-loaded nanogel (Q*c12*-NG+T) are about 254−1018-fold lower than for free Triclosan, while the MBC for Triclosan-loaded nanogel (Q*c12*-NG+T) are about 203−814-fold reduction compared to free Triclosan. All the results support the hypothesis, as shown in Scheme 1, that nanogels interacted with the peptidoglycan and cell membrane layers of Gram-positive bacteria via electrostatic interactions, and then the hydrophobic moieties punctured the cell wall and disordered the cytoplasmic membrane. This event is followed by the injection of Triclosan from the intraparticle micelles that have merged with the lipid bilayer where it damages the bacterial cell membrane further. Moreover, following the extensive membrane damage, Triclosan was injected inside the cell easily, selectively inhibiting the biosynthesis of fatty acid to stop the bacteria growth further.[36,60] Release of Triclosan will only happen when the hydrophobic moieties start to interact

https://dx.doi.org/10.1021/acsapm.0c01031
ACS Appl. Polym. Mater. 2020, 2, 5779−5789

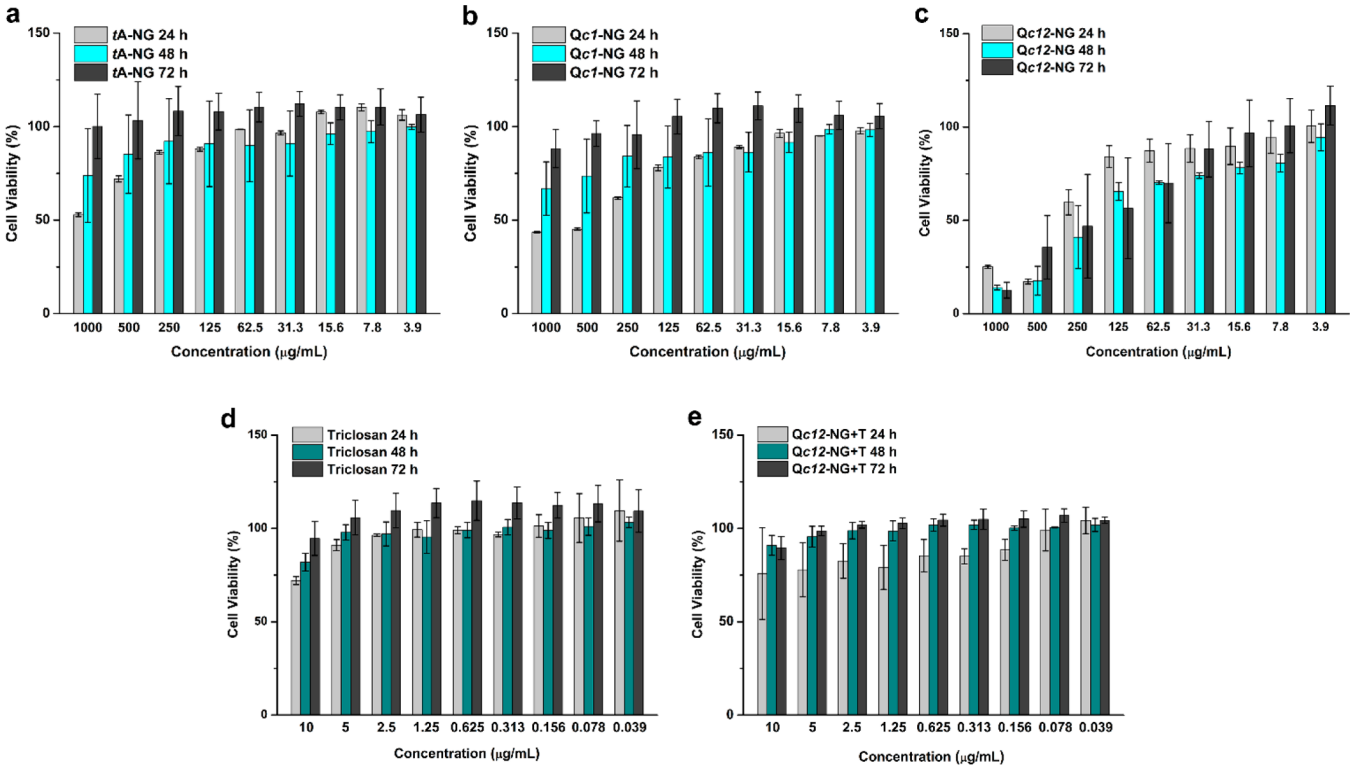

Figure 6. Cell viability in the presence of (a) tertiary amine-functionalized nanogel *t*A-NG, (b) methyl-quaternized nanogel Q*c1*-NG, (c) dodecyl-quaternized nanogel Q*c12*-NG, (d) Triclosan, and (e) Triclosan-loaded nanogel Q*c12*-NG+T. L929 fibroblasts cells were treated with nanogels and Triclosan for 24, 48, and 72 h at 37 °C, respectively. The cytotoxicity was determined by XTT assay.

with the lipid membrane resulting in a less hydrophobic environment inside the nanogel for encapsulation of Triclosan; therefore, there is no release of Triclosan outside of the membrane. This way, the effective local concentration of Triclosan dramatically increases while the overall antimicrobial agent concentration is lowering hundreds of times (Table 1 and Figure 5). Taken together, the above experimental evidence highlights that the combination of QACs-modified nanogel and hydrophobic antimicrobial agents, such as Triclosan, produces a synergistic effect via the active nanoinjection of the antimicrobial agent into the bacteria and thereby results in the extremely high bacterial killing efficiency.

Biocompatibility of Nanogels. Biocompatibility is a severe concern for any antimicrobial agent or nanocarrier that is designed to be used as a therapeutic agent. It is expected that the antibacterial drugs should possess good activity against bacteria while displaying low toxicity toward tissue cells. To investigate the biocompatibility of the prepared nanogels, the cytotoxicity was assessed using mouse fibroblast cells L929 after 24, 48, and 72 h incubation (according to ISO protocols) by XTT assay. The results are shown in Figure 6; free Triclosan was included as a control group for the comparison of Triclosan-loaded nanogel. As depicted in Figure 6a and b, after 24, 48, and 72 h incubation, the *t*A-NG had no evident influence on the cell viability at concentrations below 250 μg mL^{-1}, while the concentration of methyl-quaternized nanogel Q*c1*-NG did not display cytotoxicity below 125 μg mL^{-1}. As shown in Figure 6c, after 24 h treatment of the dodecyl-quaternized nanogel Q*c12*-NG, there is no server cytotoxicity displayed below 125 μg mL^{-1}. However, after 48 and 72 h treatment, a decrease in cell viability was observed at a concentration above 31.3 μg mL^{-1}. Compared to the bacteria-killing concentration of all these three nanogels (MBC > 250 μg mL^{-1}), the cytotoxicity toward mouse fibroblast cells is relatively high, which might be due to the damage to the cell membrane or nucleus caused by the positively charged surface of the nanogels interacting with the negatively charged lipid membrane or DNA.

In the case of free Triclosan, as shown in Figure 6d, there is no significant cytotoxicity below the concentration of 5 μg mL^{-1} after 24, 48, and 72 h treatment, which is at the same range as reported before, where Triclosan was shown to be cytotoxic to epithelial cells due to the induced stimulation of apoptosis.[61] However, to be able to kill bacteria, the required concentration of free Triclosan (MBC $\geq$ 5 μg mL^{-1}) is in a similar range as the cytotoxic concentration. Contrary to the high dose of free Triclosan needed to kill the bacteria, the concentration of Triclosan-loaded nanogel (MBC $\leq$ 0.625 μg mL^{-1} in terms of nanogel) is lower than the nontoxic concentration (2.5 μg mL^{-1} after 24 h, 10 μg mL^{-1} after 48 and 72 h, cell viability >80%, Figure 6e). Therefore, the Triclosan-loaded nanogel is more effective and more biocompatible than free Triclosan.

CONCLUSION

In this study, a quaternized nanogel system has been developed by conjugated quaternized hydrophobic moieties to the hydrophilic polymer network of the nanogel to form hydrophobic domains by intraparticle micellization of the long aliphatic chains. Then the model hydrophobic antimicrobial, Triclosan, was loaded into the hydrophobic pockets inside the nanogel network. As shown in Scheme 1, the nanogel first attaches to the bacterial cell through the positive charges

https://dx.doi.org/10.1021/acsapm.0c01031
ACS Appl. Polym. Mater. 2020, 2, 5779−5789

provided by the conjugated quaternized hydrophobic moieties to the hydrophilic polymer network of the nanogel. Release of Triclosan from the nanogel is achieved in the presence of bacteria when the hydrophobic moieties in which the Triclosan is stored interact with the lipid membrane. As the aliphatic chains intercalate and permeate the bacterial cell membrane, these do not interact as strongly anymore with Triclosan, which allows Triclosan to be liberated more easily and additionally more directly as the bacterial cell membrane is opened due to the interaction of the aliphatic QACs. The effective local concentration of Triclosan at the bacterial site is thereby dramatically increased. The minimal bactericidal concentrations become hundreds of times lower, which significantly improves the therapeutic efficacy of Triclosan. Even though Triclosan is a widely used antimicrobial agent, still it is under scrutiny because of its environmental and potential hazardous effects, which makes it important to provide systems as presented here that greatly diminish the used concentration without losing the active effects. Meanwhile, this system is promising in order to reduce the development of future bacterial resistance and lower the side effect of the antimicrobial formulation.

EXPERIMENTAL SECTION

Reagents and Chemicals. *N*-[3-(Dimethylamino)propyl]-methacrylamide (DMAPMA, 99%), 2,2′-azobis(2-methylpropioamidine)dihydrochloride (AMPA, V50, 97%), potassium carbonate (K2CO3), *N,N*′ methylene-bis(acrylamide) (BIS, 99%), hexadecyltrimethylammonium bromide (CTAB, 99%), Nile Red, methyl iodide, 1-bromododecane (97%), *N,N*-dimethylformamide (DMF, anhydrous), and deuterium oxide (D_2O) were purchased from Sigma-Aldrich, The Netherlands. *N*-Isopropylacrylamide (NIPAM, 98%) was purchased from TCI, Belgium. Potassium chloride (KCl), methanol (anhydrous), ethanol, and tetrahydrofuran (THF, anhydrous) were purchased from Merck, Germany. Triclosan was purchased from Duchefa B.V., The Netherlands. All chemicals were used as received without any further purification. Ultrapure water (18.2 MΩ, arium 611 DI water purification system; Sartorius AG, Göttingen, Germany) was used in all experiments.

Synthesis of p(NIPAM-*co*-DMAPMA) Nanogel (*t*A-NG). p(NIPAM-*co*-DMAPMA) nanogel (*t*A-NG) was synthesized as previously reported.[56] Briefly, *t*A-NG was synthesized through precipitation polymerization. To a 250 mL three-necked flask equipped with a magnetic stirrer, a reflux condenser, and a nitrogen inlet and outlet, 1.35 g (11.9 mmol, 85 mol %) of monomer NIPAM, 0.108 g (0.7 mmol, 5 mol %) of cross-linker BIS, and 0.00437 g (0.012 mmol) of surfactant CTAB were dissolved in 85 mL of water. After degassing with N_2 for 1 h by passing N_2 through the solution, the solution was heated to 85 °C, and 10 mL of 0.238 g (1.4 mmol, 10 mol %) of degassed comonomer DMAPMA solution was added with a syringe. After the pH was adjusted to 8−9 with 0.1 M HCl and 0.1 M NaOH, the reaction was started by injecting 5 mL of 0.0542 g (0.2 mmol) degassed initiator V50 solution into the reaction mixture. The reaction solution was stirred under a nitrogen atmosphere at 300 rpm for 6 h at 85 °C. The reaction mixture was cooled to room temperature and stirred overnight. The obtained nanogel was purified via ultracentrifugation (at 197 000 g for 1 h) of the dispersion and redispersion of the sediment in water (3×). The pure product was freeze-dried after purification for further use.

Quaternization of tA-NG with Methyl Iodide (Q*c1*-NG). *t*A-NG was quaternized with methyl iodide as previously reported.[56] First 0.4 g of *t*A-NG (14 wt % of amino group) and 0.058 g of K_2CO_3 were dispersed in 30.3 mL of methanol, and after the addition of 0.17 mL (2.73 mmol) of methyl iodide the reaction was started and stirred at room temperature for 4 days. Subsequently water was added to the reaction mixture, and the methanol was removed under reduced pressure. Impurities were removed via dialysis against water for 3 days (MWCO 3500 Da). The purified product Q*c1*-NG was freeze-dried for further use.

Quaternization of tA-NG with 1-Bromododecane (Q*c12*-NG). *t*A-NG was quaternized with 1-bromododecane according to a previously reported approach with a minor revision.[62] First 0.5 g (14 wt % of amino group) of *t*A-NG, 82 mg of NaOH, and 1.027 g (4.12 mmol) of 1-bromododecane were dispersed in 100 mL of DMF, and the reaction was stirred at 80 °C for 4 days. The reaction was cooled down to room temperature, and the nanogel was collected by ultracentrifugation at 197 000 g for 1 h and then further purified by dialysis against ethanol for 3 days and subsequently against water for 3 days (MWCO 3500 Da). The purified product Q*c12*-NG was freeze-dried for further use.

Preparation of Triclosan-Loaded Nanogel (Q*c12*-NG+T). To load Triclosan into Q*c12*-NG, 0.1 mL of a Triclosan solution (10 mg mL^{-1} in THF) was added to 20 mL of dispersed Q*c12*-NG (1 mg mL^{-1} in water) under stirring. The mixture was stirred overnight and subsequently dialyzed against 96% EtOH for 3 days and subsequently against water for 3 days to remove THF and unloaded Triclosan. The purified product Q*c12*-NG+T was obtained after freeze-drying.

^{1}H NMR. NMR spectra were measured with a Varian Mercury-400 NMR spectrometer (400 MHz). All spectra were measured at room temperature. D_2O was used as a solvent, and a nanogel concentration of 10 mg mL^{-1} was used. The chemical shifts are presented in parts per million downfield from the TMS standard. The proton signal of residual D_2O was used as a reference.

Transmission Electron Microscopy (TEM). The morphologies of the nanogels were observed under a Philips CM120 Microscope coupled to a 4k CCD camera using an acceleration voltage of 120 kV. All the samples were negatively stained with uranyl acetate and drop casted on a carbon film coated Cu grid.

Temperature-Dependent Dynamic Light Scattering and Zeta Potential (ζ) Measurements. The hydrodynamic radius (R_h) and polydispersities of the nanogels were determined by dynamic light scattering (DLS). The measurements were performed using a Malvern ZetaSizer ZS ZEN3600 (Malvern Instruments, U.K.) equipped with a temperature controller. The scattering detector was positioned at a fixed scattering angle of 173°. The concentrations of nanogel dispersions were around 0.1 mg mL^{-1} in water. Hydrodynamic radii were calculated from the diffusion coefficients using the Stokes−Einstein equation. The polydispersity index is given by the cumulant analysis method. Temperature-dependent measurements were performed in a range of 20−60 °C with 2 °C intervals. Before the data collection of each temperature, the sample was allowed to equilibrate for 3 min at the proper temperature. Each data point is an average of three successive size measurements, which themselves consist of 11−15 measurements.

Zeta potential measurements were performed with the same instrument. The concentrations of nanogel dispersions were around 0.01 mg mL^{-1}. The ζ-potentials were a result of the average of three successive measurements. All nanogel solutions used for pH-dependent ζ-potential measurements were diluted with 0.05 M NaCl and adjusted to the desired pH (pH 3−11) with 0.1 M HCl and/or 0.1 M NaOH.

Fluorescence Spectroscopy. To prove that the hydrophobic cavities were formed from the aliphatic chains of 1-bromododecane in Q*c12*-NG, Nile Red, a model hydrophobic dye, was incorporated into Q*c12*-NG in the same way as Triclosan. For comparison reasons a dye-containing dispersion made of the *t*A-NG without aliphatic chains was prepared. After purification, 1 mL of Nile Red-loaded Q*c12*-NG and *t*A-NG was dispersed in water (0.1 mg mL^{-1}) for fluorescence measurement. The fluorescence spectroscopy was performed at 24 °C using a SpectraMax M3Multi-Mode Plate Reader at an excitation wavelength of 540 nm (emission wavelength from 590 to 700 nm in 10 nm steps). Water was used as a reference.

The fluorescence spectra of Triclosan and Triclosan-loaded nanogel were collected using the same method at an excitation wavelength of 280 nm (emission wavelength from 295 to 470 nm in 10 nm steps).

https://dx.doi.org/10.1021/acsapm.0c01031
ACS Appl. Polym. Mater. 2020, 2, 5779−5789

UV−Vis Spectroscopy. The Triclosan loading content of Q*c12*-NG+T was measured by UV−vis spectroscopy. The absorbance of the nanogel solution at 280 nm was recorded on a UV−vis spectrophotometer (PerkinElmer Lambda 2s). With the use of a calibration curve obtained over a series of Triclosan concentrations (1.25, 2.5, 5, 10, 20, and 40 μg mL^{-1}), the UV absorbance was correlated to the amounts of Triclosan that were loaded in the nanogel by isolating the signal of the Triclosan via deconvolution.

Bacterial Strain and Growth Conditions. Four bacterial strains were used in this study: *S. aureus* ATCC 12600, *S. aureus* 5298, *S. epidermidis* ATCC 12228, and *S. epidermidis* HBH 45. All strains were first cultured from cryopreservative beads onto a blood agar plate overnight at 37 °C in ambient air. For experiments, one colony was transferred to inoculate 10 mL of tryptone soya broth (TSB for *S. aureus* ATCC 12600 and *S. aureus* 5298; OXOID LTD, U.K.) or nutrient broth (NB for *S. epidermidis* ATCC 12228 and *S. epidermidis* HBH 45; OXOID LTD, U.K.) at 37 °C for 24 h in ambient air. This preculture was then used to inoculate a second culture of 200 mL of TSB or NB and grown statically for 16−18 h at 37 °C. The bacteria from the second culture were harvested by centrifugation at 5000 g for 5 min at 10 °C and washed twice with potassium phosphate buffered saline (PBS, 10 mM potassium phosphate, 0.15 M NaCl, pH 7.0). Subsequently, bacteria were sonicated for 30 s at 30 W (Vibra Cell model VCX130; Sonics and Materials Inc., Newtown, CT) while cooling in an ice/water bath to obtain single bacteria by breaking possible bacterial aggregates. Finally, the bacteria were resuspended in 200 mL of TSB or NB to a concentration of 1×10^5 bacteria mL^{-1} as detected using a Bürker−Türk counting chamber.

Antimicrobial Properties. The antimicrobial properties of quaternized nanogels Q*c1*-NG and Q*c12*-NG and Triclosan-loaded nanogel Q*c12*-NG+T against planktonic staphylococci were evaluated by determining the minimal inhibitory (MIC) and minimal bactericidal concentrations (MBC). The nonquaternized *t*A-NG and Triclosan were tested as control groups. Nanogels and Triclosan were dispersed in either TSB or NB and further serial diluted in 96-well plates (100 μL per well) except the positive control wells containing only broth medium. Ten microliters of the above-mentioned bacterial suspension (1×10^5 bacteria mL^{-1}) was added to each well and incubated for 24 h at 37 °C. All these growth assays were performed in triplicate. To obtain a higher and homogeneous solubility in TSB or NB medium, we first dissolved Triclosan in ethanol, and then diluted it with the medium to get a solubility of 20 mg/L in a 1:50 solution of ethanol:TSB/NB medium (pH 7.2). This approach results in a homogeneous Triclosan solution of 20 mg/L in the medium at 37 °C.

The MIC values were taken at the lowest concentration of nanogels or Triclosan at which no visual bacterial growth was detectable. The MBC values were determined by plating each MIC dilution series of no visible bacteria growth on TSB or NB agar plates. After being incubated for 24 h at 37 °C, the lowest concentration at which colony formation remained absent was taken as the MBC. Three independent experiments were performed for each sample tested.

Cytotoxicity Assay. XTT assay was carried out to evaluate the cytotoxicity of nanogels against L929 cells (Mouse fibroblast cell line). Triclosan was selected as a control. L929 cells were cultured in Minimum Essential Medium (MEM, Gibco) supplemented with 10% fetal bovine serum (Gibco) and 100 units mL^{-1} of streptomycin and penicillin (Gibco). The cells were maintained at 37 °C in a humidified atmosphere of 5% CO_2 in air. L929 cells were separately seeded into 96-well plates at a density of 8000 cells per well for 24 h and 5000 cells per well for 48 and 72 h (n = 3). Wells containing 100 μL of medium alone were included as blank absorbance readings. After 24 h of incubation, the medium was replaced with 100 μL of fresh medium containing nanogels and Triclosan at various concentrations (1000, 500, 250, 125, 62.5, 31.3, 15.6, 7.8, and 3.9 μg mL^{-1} for *t*A-NG, Q*c1*-NG, and Q*c12*-NG; 10, 5, 2.5, 1.25, 0.625, 0.313, 0.156, 0.078, and 0.039 μg mL^{-1} for Q*c12*-NG+T and Triclosan) and incubated for another 24, 48, or 72 h. Cells without treatment were used as the control. Afterward, 50 μL of XTT solution (2,3-bis(2-methoxy-4-nitro-5-sulfophenyl)-2*H*-tetrazolium-5-carboxanilide, AppliChem, A8088) was added to each well, and the cells were then incubated for another 2 h. The absorbance at 490 nm was measured with a FluoStar Optima Plate reader. To avoid nonspecific readings, the absorbance at 690 nm was measured and subtracted from the 490 nm measurement. The cell viability was determined by the standard XTT assay protocols. Three independent experiments were performed for each sample tested.

■ ASSOCIATED CONTENT

Supporting Information

The Supporting Information is available free of charge at https://pubs.acs.org/doi/10.1021/acsapm.0c01031.

^{1}H NMR spectra of *t*A-NG, Q*c1*-NG, and Q*c12*-NG, UV−vis absorbance as a function of Triclosan concentration, and UV−vis absorption spectra of Triclosan and Triclosan loaded nanogel Q*c12*-NG+T (PDF)

■ AUTHOR INFORMATION

Corresponding Authors

Patrick van Rijn − *Department of Biomedical Engineering, W. J. Kolff Institute for Biomedical Engineering and Materials Science, University of Groningen and University Medical Center Groningen, 9713 AV Groningen, The Netherlands;* orcid.org/0000-0002-2208-5725; Email: p.van.rijn@umcg.nl

Olga Mergel − *Department of Biomedical Engineering, W. J. Kolff Institute for Biomedical Engineering and Materials Science, University of Groningen and University Medical Center Groningen, 9713 AV Groningen, The Netherlands;* Email: Olga.Mergel@rwth-aachen.de

Authors

Guangyue Zu − *Department of Biomedical Engineering, W. J. Kolff Institute for Biomedical Engineering and Materials Science, University of Groningen and University Medical Center Groningen, 9713 AV Groningen, The Netherlands;* orcid.org/0000-0001-5252-8876

Magdalena Steinmüller − *Department of Biomedical Engineering, W. J. Kolff Institute for Biomedical Engineering and Materials Science, University of Groningen and University Medical Center Groningen, 9713 AV Groningen, The Netherlands*

Damla Keskin − *Department of Biomedical Engineering, W. J. Kolff Institute for Biomedical Engineering and Materials Science, University of Groningen and University Medical Center Groningen, 9713 AV Groningen, The Netherlands*

Henny C. van der Mei − *Department of Biomedical Engineering, W. J. Kolff Institute for Biomedical Engineering and Materials Science, University of Groningen and University Medical Center Groningen, 9713 AV Groningen, The Netherlands;* orcid.org/0000-0003-0760-8900

Complete contact information is available at: https://pubs.acs.org/10.1021/acsapm.0c01031

Author Contributions

The manuscript was written through contributions of all authors. All authors have given approval to the final version of the manuscript.

Funding

G.Z. is funded by the China Scholarship Council (CSC; G.Z no.201706890012). O.M. is funded by the Alexander von Humboldt Foundation being awarded the Feodor Lynen

Research Fellowship. D.K. has received funding from the European Union's Horizon 2020 research and innovation program under the Marie Skłodowska-Curie grant agreement No. 713482 (ALERT program).

Notes

The authors declare the following competing financial interest(s): P.v.R also is co-founder, scientific advisor, and share-holder of BiomACS BV, a biomedical oriented screening company.

REFERENCES

(1) Mendoza, N.; Ravanfar, P.; Satyaprakah, A.; Pillai, S.; Creed, R. Existing Antibacterial Vaccines. *Dermatol. Ther.* **2009**, *22*, 129−142.
(2) Holmes, A. H.; Moore, L. S. P.; Sundsfjord, A.; Steinbakk, M.; Regmi, S.; Karkey, A.; Guerin, P. J.; Piddock, L. J. V. Understanding the Mechanisms and Drivers of Antimicrobial Resistance. *Lancet* **2016**, *387*, 176−187.
(3) Burnham, C. A. D.; Leeds, J.; Nordmann, P.; O'Grady, J.; Patel, J. Diagnosing Antimicrobial Resistance. *Nat. Rev. Microbiol.* **2017**, *15*, 697−703.
(4) Laxminarayan, R.; Matsoso, P.; Pant, S.; Brower, C.; Røttingen, J. A.; Klugman, K.; Davies, S. Access to Effective Antimicrobials: A Worldwide Challenge. *Lancet* **2016**, *387*, 168−175.
(5) Levy, S. B.; Marshall, B. Antibacterial Resistance Worldwide: Causes, Challenges and Responses. *Nat. Med.* **2004**, *10*, S122−S129.
(6) Wang, L.; Hu, C.; Shao, L. The Antimicrobial Activity of Nanoparticles: Present situation and Prospects for the Future. *Int. J. Nanomed.* **2017**, *12*, 1227−1249.
(7) Loher, S.; Schneider, O. D.; Maienfisch, T.; Bokorny, S.; Stark, W. J. Micro-Organism-Triggered Release of Silver Nanoparticles from Biodegradable Oxide Carriers Allows Preparation of Self-Sterilizing Polymer Surfaces. *Small* **2008**, *4*, 824−832.
(8) Marambio-Jones, C.; Hoek, E. M. V. A Review of the Antibacterial Effects of Silver Nanomaterials and Potential Implications for Human Health and the Environment. *J. Nanopart. Res.* **2010**, *12*, 1531−1551.
(9) Mokabber, T.; Cao, H. T.; Norouzi, N.; Van Rijn, P.; Pei, Y. T. Antimicrobial Electrodeposited Silver-Containing Calcium Phosphate Coatings. *ACS Appl. Mater. Interfaces* **2020**, *12*, 5531−5541.
(10) Ren, G.; Hu, D.; Cheng, E. W. C.; Vargas-Reus, M. A.; Reip, P.; Allaker, R. P. Characterisation of Copper Oxide Nanoparticles for Antimicrobial Applications. *Int. J. Antimicrob. Agents* **2009**, *33*, 587−590.
(11) Zhao, Y.; Tian, Y.; Cui, Y.; Liu, W.; Ma, W.; Jiang, X. Small Molecule-Capped Gold Nanoparticles as Potent Antibacterial Agents That Target Gram-Negative Bacteria. *J. Am. Chem. Soc.* **2010**, *132*, 12349−12356.
(12) Zou, X.; Zhang, L.; Wang, Z.; Luo, Y. Mechanisms of the Antimicrobial Activities of Graphene Materials. *J. Am. Chem. Soc.* **2016**, *138*, 2064−2077.
(13) Sun, H.; Gao, N.; Dong, K.; Ren, J.; Qu, X. Graphene Quantum Dots-Band-Aids Used for Wound Disinfection. *ACS Nano* **2014**, *8*, 6202−6210.
(14) Liu, L.; Xu, K.; Wang, H.; Jeremy Tan, P. K.; Fan, W.; Venkatraman, S. S.; Li, L.; Yang, Y.-Y. Self-Assembled Cationic Peptide Nanoparticles as An Efficient Antimicrobial Agent. *Nat. Nanotechnol.* **2009**, *4*, 457.
(15) Ong, Z. Y.; Wiradharma, N.; Yang, Y. Y. Strategies Employed in the Design and Optimization of Synthetic Antimicrobial Peptide Amphiphiles with Enhanced Therapeutic Potentials. *Adv. Drug Delivery Rev.* **2014**, *78*, 28−45.
(16) Friedman, A. J.; Phan, J.; Schairer, D. O.; Champer, J.; Qin, M.; Pirouz, A.; Blecher-Paz, K.; Oren, A.; Liu, P. T.; Modlin, R. L.; Kim, J. Antimicrobial and Anti-Inflammatory Activity of Chitosan-Alginate Nanoparticles: A Targeted Therapy for Cutaneous Pathogens. *J. Invest. Dermatol.* **2013**, *133*, 1231−1239.
(17) Dong, X.; Awak, M. A.; Tomlinson, N.; Tang, Y.; Sun, Y. P.; Yang, L. Antibacterial Effects of Carbon Dots in Combination with Other Antimicrobial Reagents. *PLoS One* **2017**, *12*, e0185324.
(18) Makvandi, P.; Jamaledin, R.; Jabbari, M.; Nikfarjam, N.; Borzacchiello, A. Antibacterial Quaternary Ammonium Compounds in Dental Materials: A Systematic Review. *Dent. Mater.* **2018**, *34*, 851−867.
(19) Tomlinson, E.; Brown, M. R. W.; Davis, S. S. Effect of Colloidal Association on the Measured Activity of Alkylbenzyldimethylammonium Chlorides against Pseudomonas Aeruginosa. *J. Med. Chem.* **1977**, *20*, 1277−1282.
(20) Hamilton, W. A. The Mechanism of the Bacteriostatic Action of Tetrachlorosalicylanilide: A Membrane-Active Antibacterial Compound. *J. Gen. Microbiol.* **1968**, *50*, 441−458.
(21) Ioannou, C. J.; Hanlon, G. W.; Denyer, S. P. Action of Disinfectant Quaternary Ammonium Compounds against Staphylococcus Aureus. *Antimicrob. Agents Chemother.* **2007**, *51*, 296−306.
(22) Jennings, M. C.; Minbiole, K. P. C.; Wuest, W. M. Quaternary Ammonium Compounds: An Antimicrobial Mainstay and Platform for Innovation to Address Bacterial Resistance. *ACS Infect. Dis.* **2015**, *1*, 288−303.
(23) Kenawy, E. R.; Worley, S. D.; Broughton, R. The Chemistry and Applications of Antimicrobial Polymers: A State-of-the-Art Review. *Biomacromolecules* **2007**, *8*, 1359−1384.
(24) Waschinski, C. J.; Herdes, V.; Schueler, F.; Tiller, J. C. Influence of Satellite Groups on Telechelic Antimicrobial Functions of Polyoxazolines. *Macromol. Biosci.* **2005**, *5*, 149−156.
(25) Loontjens, J. A. Quaternary Ammonium Compounds. In *Biomaterials Associated Infection: Immunological Aspects and Antimicrobial Strategies*; Springer: New York, 2013; pp 379−404.
(26) Wei, T.; Tang, Z.; Yu, Q.; Chen, H. Smart Antibacterial Surfaces with Switchable Bacteria-Killing and Bacteria-Releasing Capabilities. *ACS Appl. Mater. Interfaces* **2017**, *9*, 37511−37523.
(27) Piras, A. M.; Esin, S.; Benedetti, A.; Maisetta, G.; et al. Antibacterial, Antibiofilm, and Antiadhesive Properties of Different Quaternized Chitosan Derivatives. *Int. J. Mol. Sci.* **2019**, *20*, 6297.
(28) Sun, B.; Xi, Z.; Wu, F.; Song, S.; Huang, X.; Chu, X.; Wang, Z.; Wang, Y.; Zhang, Q.; Meng, N.; Zhou, N.-L.; Shen, J. Quaternized Chitosan-Coated Montmorillonite Interior Antimicrobial Metal−Antibiotic in Situ Coordination Complexation for Mixed Infections of Wounds. *Langmuir* **2019**, *35*, 15275−15286.
(29) Wen, Y.; Yao, F.; Sun, F.; Tan, Z.; Tian, L.; Xie, L.; Song, Q. Antibacterial Action Mode of Quaternized Carboxymethyl Chitosan/Poly(Amidoamine) Dendrimer Core-Shell Nanoparticles against Escherichia Coli Correlated with Molecular Chain Conformation. *Mater. Sci. Eng., C* **2015**, *48*, 220−227.
(30) Inam, M.; Foster, J. C.; Gao, J.; Hong, Y.; Du, J.; Dove, A. P.; O'Reilly, R. K. Size and Shape Affects the Antimicrobial Activity of Quaternized Nanoparticles. *J. Polym. Sci., Part A: Polym. Chem.* **2019**, *57*, 255−259.
(31) Dong, H.; Huang, J.; Koepsel, R. R.; Ye, P.; Russell, A. J.; Matyjaszewski, K. Recyclable Antibacterial Magnetic Nanoparticles Grafted with Quaternized Poly(2-(Dimethylamino)Ethyl Methacrylate) Brushes. *Biomacromolecules* **2011**, *12*, 1305−1311.
(32) Zhang, X.; Chen, X.; Yang, J.; Jia, H. R.; Li, Y. H.; Chen, Z.; Wu, F. G. Quaternized Silicon Nanoparticles with Polarity-Sensitive Fluorescence for Selectively Imaging and Killing Gram-Positive Bacteria. *Adv. Funct. Mater.* **2016**, *26*, 5958−5970.
(33) Ferreira, C.; Pereira, A. M.; Pereira, M. C.; Melo, L. F.; Simões, M. Physiological Changes Induced by the Quaternary Ammonium Compound Benzyldimethyldodecylammonium Chloride on Pseudomonas Fluorescens. *J. Antimicrob. Chemother.* **2011**, *66*, 1036−1043.
(34) Ahlström, B.; Thompson, R. A.; Edebo, L. The Effect of Hydrocarbon Chain Length, PH, and Temperature on the Binding and Bactericidal Effect of Amphiphilic Betaine Esters on Salmonella Tvphimurium. *Apmis* **1999**, *107*, 318−324.
(35) Jeong, D.; Joo, S. W.; Shinde, V. V.; Cho, E.; Jung, S. Carbohydrate-Based Host-Guest Complexation of Hydrophobic

https://dx.doi.org/10.1021/acsapm.0c01031
ACS Appl. Polym. Mater. 2020, 2, 5779−5789

Antibiotics for the Enhancement of Antibacterial Activity. *Molecules* **2017**, *22*, 1311.
(36) McMurry, L. M.; Oethinger, M.; Levy, S. B. Triclosan Targets Lipid Synthesis. *Nature* **1998**, *394*, 531−532.
(37) Hajebi, S.; Rabiee, N.; Bagherzadeh, M.; Ahmadi, S.; Rabiee, M.; Roghani-Mamaqani, H.; Tahriri, M.; Tayebi, L.; Hamblin, M. R. Stimulus-Responsive Polymeric Nanogels as Smart Drug Delivery Systems. *Acta Biomater.* **2019**, *92*, 1−18.
(38) Karg, M.; Pich, A.; Hellweg, T.; Hoare, T.; Lyon, L. A.; Crassous, J. J.; Suzuki, D.; Gumerov, R. A.; Schneider, S.; Potemkin, I. I.; Richtering, W. Nanogels and Microgels: From Model Colloids to Applications, Recent Developments, and Future Trends. *Langmuir* **2019**, *35*, 6231−6255.
(39) Cao, Z.; Zhou, X.; Wang, G. Selective Release of Hydrophobic and Hydrophilic Cargos from Multi-Stimuli-Responsive Nanogels. *ACS Appl. Mater. Interfaces* **2016**, *8*, 28888−28896.
(40) Yang, H.; Wang, Q.; Huang, S.; Xiao, A.; Li, F.; Gan, L.; Yang, X. Smart PH/Redox Dual-Responsive Nanogels for On-Demand Intracellular Anticancer Drug Release. *ACS Appl. Mater. Interfaces* **2016**, *8*, 7729−7738.
(41) Gu, Z.; Dang, T. T.; Ma, M.; Tang, B. C.; Cheng, H.; Jiang, S.; Dong, Y.; Zhang, Y.; Anderson, D. G. Glucose-Responsive Microgels Integrated with Enzyme Nanocapsules for Closed-Loop Insulin Delivery. *ACS Nano* **2013**, *7*, 6758−6766.
(42) Agrawal, G.; Schürings, M. P.; Van Rijn, P.; Pich, A. Formation of Catalytically Active Gold-Polymer Microgel Hybrids via A Controlled in Situ Reductive Process. *J. Mater. Chem. A* **2013**, *1*, 13244−13251.
(43) Keskin, D.; Mergel, O.; Van Der Mei, H. C.; Busscher, H. J.; Van Rijn, P. Inhibiting Bacterial Adhesion by Mechanically Modulated Microgel Coatings. *Biomacromolecules* **2019**, *20*, 243−253.
(44) Brosel-Oliu, S.; Mergel, O.; Uria, N.; Abramova, N.; Van Rijn, P.; Bratov, A. 3D Impedimetric Sensors as A Tool for Monitoring Bacterial Response to Antibiotics. *Lab Chip* **2019**, *19*, 1436−1447.
(45) Kim, D. J.; Jeon, T. Y.; Baek, Y. K.; Park, S. G.; Kim, D. H.; Kim, S. H. Metal Nanoparticle-Loaded Microgels with Selective Permeability for Direct Detection of Small Molecules in Biological Fluids. *Chem. Mater.* **2016**, *28*, 1559−1565.
(46) Mergel, O.; Schneider, S.; Tiwari, R.; Kühn, P. T.; Keskin, D.; Stuart, M. C. A.; Schöttner, S.; De Kanter, M.; Noyong, M.; Caumanns, T.; Mayer, J.; Janzen, C.; Simon, U.; Gallei, M.; Wöll, D.; Van Rijn, P.; Plamper, F. A. Cargo Shuttling by Electrochemical Switching of Core-Shell Microgels Obtained by A Facile One-Shot Polymerization. *Chem. Sci.* **2019**, *10*, 1844−1856.
(47) Weldrick, P. J.; Hardman, M. J.; Paunov, V. N. Enhanced Clearing of Wound-Related Pathogenic Bacterial Biofilms Using Protease-Functionalized Antibiotic Nanocarriers. *ACS Appl. Mater. Interfaces* **2019**, *11*, 43902−43919.
(48) Bao, Q.; Zhang, D.; Qi, P. Synthesis and Characterization of Silver Nanoparticle and Graphene Oxide Nanosheet Composites as A Bactericidal Agent for Water Disinfection. *J. Colloid Interface Sci.* **2011**, *360*, 463−470.
(49) Barth, E.; Myrvik, Q. M.; Wagner, W.; Gristina, A. G. In Vitro and in Vivo Comparative Colonization of Staphylococcus Aureus and Staphylococcus Epidermidis on Orthopaedic Implant Materials. *Biomaterials* **1989**, *10*, 325−328.
(50) Chessa, D.; Ganau, G.; Spiga, L.; Bulla, A.; Mazzarello, V.; Campus, G. V.; Rubino, S. Staphylococcus Aureus and Staphylococcus Epidermidis Virulence Strains as Causative Agents of Persistent Infections in Breast Implants. *PLoS One* **2016**, *11*, e0146668−15.
(51) Greenspan, P.; Fowler, S. D. Spectrofluorometric Studies of the Lipid Probe, Nile Red. *J. Cell Biol.* **1985**, *26*, 781−789.
(52) Jiang, J.; Qi, B.; Lepage, M.; Zhao, Y. Polymer Micelles Stabilization on Demand through Reversible Photo-Cross-Linking. *Macromolecules* **2007**, *40*, 790−792.
(53) Rumin, J.; Bonnefond, H.; Saint-Jean, B.; Rouxel, C.; Sciandra, A.; Bernard, O.; Cadoret, J. P.; Bougaran, G. The Use of Fluorescent Nile Red and BODIPY for Lipid Measurement in Microalgae. *Biotechnology for Biofuels*; BioMed Central Ltd.: London, U.K., March 12, 2015; p 42.
(54) Greenspan, P.; Mayer, E. P.; Fowler, S. D. Nile Red: A Selective Fluorescent Stain for Intracellular Lipid Droplets. *J. Cell Biol.* **1985**, *100*, 965−973.
(55) Zou, L.; Mi, C.; Yu, H.; Gu, W.; Teng, Y. Characterization of the Interaction between Triclosan and Catalase. *RSC Adv.* **2017**, *7*, 9031−9036.
(56) Mergel, O.; Gelissen, A. P. H.; Wünnemann, P.; Böker, A.; Simon, U.; Plamper, F. A. Selective Packaging of Ferricyanide within Thermoresponsive Microgels. *J. Phys. Chem. C* **2014**, *118*, 26199−26211.
(57) Ramos, J.; Imaz, A.; Forcada, J. Temperature-Sensitive Nanogels: Poly(N-Vinylcaprolactam) versus Poly(N-Isopropylacrylamide). *Polym. Chem.* **2012**, *3*, 852−856.
(58) Gelissen, A. P. H.; Schmid, A. J.; Plamper, F. A.; Pergushov, D. V.; Richtering, W. Quaternized Microgels as Soft Templates for Polyelectrolyte Layer-by-Layer Assemblies. *Polymer* **2014**, *55*, 1991−1999.
(59) Liu, Y.; Busscher, H. J.; Zhao, B.; Li, Y.; Zhang, Z.; Van Der Mei, H. C.; Ren, Y.; Shi, L. Surface-Adaptive, Antimicrobially Loaded, Micellar Nanocarriers with Enhanced Penetration and Killing Efficiency in Staphylococcal Biofilms. *ACS Nano* **2016**, *10*, 4779−4789.
(60) Slater-Radosti, C. Biochemical and Genetic Characterization of the Action of Triclosan on Staphylococcus Aureus. *J. Antimicrob. Chemother.* **2001**, *48*, 1−6.
(61) Zuckerbraun, H. L.; Babich, H.; May, R.; Sinensky, M. C. Triclosan, Cytotoxicity, Mode of Action, and Induction of Apoptosis in Human Gingival Cells in Vitro. *Eur. J. Oral Sci.* **1998**, *106*, 628−636.
(62) Yue, J.; Zhao, P.; Gerasimov, J. Y.; Van De Lagemaat, M.; Grotenhuis, A.; Rustema-Abbing, M.; Van Der Mei, H. C.; Busscher, H. J.; Herrmann, A.; Ren, Y. 3D-Printable Antimicrobial Composite Resins. *Adv. Funct. Mater.* **2015**, *25*, 6756.

https://dx.doi.org/10.1021/acsapm.0c01031
ACS Appl. Polym. Mater. 2020, 2, 5779−5789